

Extracting Higher Order Critical Points and Topological Simplification of 3D Vector Fields

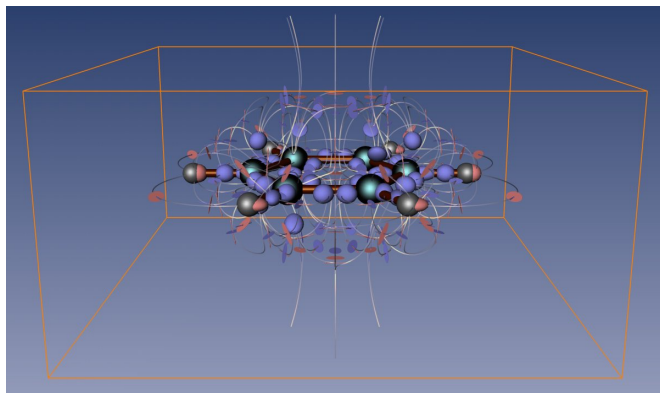
Tino Weinkauff*
ZIB Berlin

Holger Theisel†
MPI Saarbrücken

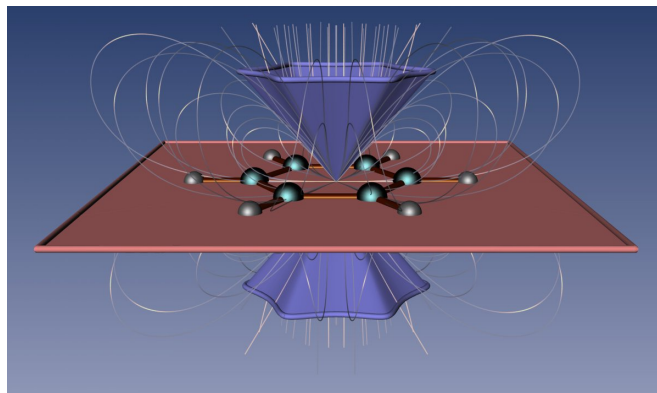
Kuangyu Shi‡
MPI Saarbrücken

Hans-Christian Hege§
ZIB Berlin

Hans-Peter Seidel¶
MPI Saarbrücken



(a) 184 first order critical points. The box around the molecule represents the chosen area for topological simplification.



(b) Topologically simplified representation with one higher order critical point elucidates the far field behavior of the benzene.

Figure 1: Topological representations of the electrostatic field of the benzene molecule.

ABSTRACT

This paper presents an approach to extracting and classifying higher order critical points of 3D vector fields. To do so, we place a closed convex surface s around the area of interest. Then we show that the complete 3D classification of a critical point into areas of different flow behavior is equivalent to extracting the topological skeleton of an appropriate 2D vector field on s , if each critical point is equipped with an additional Bit of information. Out of this skeleton, we create an icon which replaces the complete topological structure inside s for the visualization. We apply our method to find a simplified visual representation of clusters of critical points, leading to expressive visualizations of topologically complex 3D vector fields.

CR Categories: I.3.3 [Computer Graphics]: Line and Curve Generation I.3.7 [Computer Graphics]: Three-Dimensional Graphics and Realism

1 INTRODUCTION

Topological methods have become a standard tool to visualize 2D and 3D vector fields because they offer to represent a complex flow behavior by only a limited number of graphical primitives. [6] introduced them as a visualization tool by extracting critical points and classifying them into sources, sinks and saddles, and integrat-

ing certain stream lines called separatrices from the saddles in the directions of the eigenvectors of the Jacobian matrix. Later, topological methods have been extended to higher order critical points [12], boundary switch points [2], and closed separatrices [22]. In addition, topological methods have been applied to simplify [2] [3] [17] [18], smooth [21], compress [7] and design [15] vector fields. The topology of 3D vector fields is visualized in [5], [8], [9], [16], [19]. [11] gives an overview on flow visualization techniques focusing on feature extraction approaches.

In general we see that there is still a rather small amount of research done for topological methods of 3D vector fields. Similar to 2D vector fields, 3D vector fields can have higher order critical points. Also, there can be clusters of critical points which should be combined to a more simple representation.

In this paper we present an approach to extracting higher order critical points of 3D vector fields which can be used as a topological simplification method. Although the extraction of higher order critical points [12] and the topological simplification [17] are well-researched for 2D vector fields, we are not aware of any topological simplification or higher order critical point extraction approaches for 3D vector fields.

The solution which we present here can be considered as a 3D extension of [17]. There, a convex closed polygon is placed around an area of interest (i.e., a cluster of critical points) and the potential location \mathbf{c} of the higher order critical point is set inside the polygon. Then a segmentation into areas of different flow behavior is achieved by analyzing number and order of the points \mathbf{x} on the polygon where the vector of the vector field is either parallel or perpendicular to $\mathbf{x} - \mathbf{c}$.

Similar to [17], our solution for a 3D vector field \mathbf{v} first assumes that the location of a higher order critical point is known. Then a closed convex surface s with genus zero is placed around \mathbf{c} , and the topological classification of \mathbf{c} is achieved by analyzing the flow behavior towards \mathbf{c} for stream lines starting from each point of s . The

*e-mail: weinkauff@zib.de

†e-mail: theisel@mpi-inf.mpg.de

‡e-mail: skyshi@mpi-inf.mpg.de

§e-mail: hege@zib.de

¶e-mail: hpseidel@mpi-inf.mpg.de

result is a segmentation of s into areas of different flow behavior around c . For this, an icon is created which represents the higher order critical point in the visualization.

Although this approach primarily assumes that s surrounds a very small area around a critical point, it can also be used to cover larger areas, for instance clusters of critical points. In this case, the location of the critical point c has to be set inside s (for instance at the average position of all critical points inside s). Then the result is an icon for a higher order critical point which replaces the complete topological skeleton of the area inside s in the visualization. This way the algorithm acts as a topological simplification technique.

This paper can also be seen as an extension of [10] which puts a closed surface around a region of interest as well in order to compute the index of the circumscribed area by an geometric algebra approach. However, our approach does not focus on the index of a critical point but on segmentation of areas of different flow behavior. Also, [10] mainly aims in the detection of critical points while our approach is applied to simplify 3D vector fields.

The rest of the paper is organized as follows: section 2 gives a short overview about the topological behavior around general 3D critical points. Section 3 gives the main theoretical contribution of the paper. It shows that the complete segmentation of a 3D critical point can be done by extracting the topological skeleton of a suitable 2D vector field on a closed surface where each critical point is equipped with an additional Bit of information. While section 4 presents an appropriate icon for 3D higher order critical points, section 5 applies our method to simplify a topologically complex vector field. Section 6 draws conclusions and mentions issues for future research.

2 THE TOPOLOGY OF A 3D CRITICAL POINT

Given is a 3D vector field \mathbf{v} which has an isolated critical point c . This means that $\mathbf{v}(c) = (0, 0, 0)^T$, and $\mathbf{v}(x) \neq (0, 0, 0)^T$ in a certain neighborhood of c . If the Jacobian at c fulfills $\det(\mathbf{J}(c)) \neq 0$, c is a first order critical point which can be classified as a source, sink or saddle by an eigenvalue/eigenvector-analysis of \mathbf{J} (see [19] for details).

In this paper we are particularly interested in higher order critical points, i.e. critical points with $\det(\mathbf{J}(c)) = 0$. To capture the topological behavior of such a point c , we consider a small closed surface s around c which has as well-defined surface normal almost everywhere. A variety of different shapes for s can be chosen. For the theoretical explanation in this section we use a sphere, whereas later for the introduction of our algorithm we use a box. In order to capture the topology of c only, the surface s has to be chosen that small that the flow at any point on s is governed by c . In particular, no other critical point except c must be inside s . Then every point x on s can be classified by considering the stream line of \mathbf{v} starting in x in both forward and backward direction. In one of those directions the stream line can have two kinds of behavior concerning c : it may run into c , or it may diverge away from c . Then x can be classified in the following way:

- x belongs to an *inflow sector* (parabolic) if the forward integration of \mathbf{v} from x ends in c while the backward integration diverges away from c .
- x belongs to an *outflow sector* (parabolic) if the forward integration diverges away from c and the backward integration ends in c .
- x belongs to a *hyperbolic sector* if both forward and backward integration diverge away from c .
- x belongs to a *elliptic sector* if both forward and backward integration end in c .

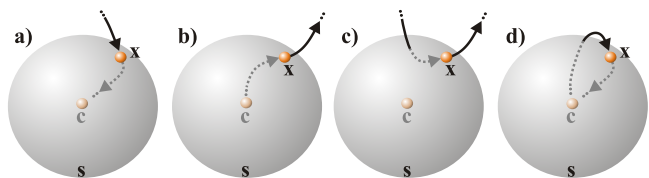


Figure 2: F-classification of x concerning the behavior of the stream line in forward and backward direction: x belongs to a) an inflow sector, b) an outflow sector, c) a hyperbolic sector, d) an elliptic sector.

forward integration	backward integration	F-classification	color scheme
ends in c	diverges from c	inflow	blue
diverges from c	ends in c	outflow	red
diverges from c	diverges from c	hyperbolic	yellow
ends in c	ends in c	elliptic	green

Table 1: F-Classification: 3D flow behavior of a stream line with respect to c .

In the following we call this classification the *F-classification* of x . "F" stands for flow because we analyze where the flow (both in forward and backward direction) starting from a point converges to. Figure 2 gives an illustration, whereas table 1 summarizes it. This table already introduces the color coding which later will be used to visualize areas of different F-classification. Note that for a classification of a point $x \in s$ it is not sufficient to check whether $\mathbf{v}(x)$ points inside or outside s . Figure 3a shows an example where $\mathbf{v}(x)$ points outside s while the stream line integration starting from x yields that x is part of an inflow sector.

Now a topological segmentation of c simply means to find a segmentation on s into areas of different F-classification. To do so, certain separation curves on s have to be extracted. These are curves with the property that all points on them have the same F-classification, while the adjacent points on at least one side of the curve have another F-classification. Examples of separation curves are shown in figure 3b. Here the red and blue closed lines on s separate a hyperbolic sector from an inflow sector and an outflow sector respectively.

For the Computer Graphics community, a first approach to treat sectors of different flow behavior around 3D critical points was given in [20]. However, this approach did not consider the extraction but the construction of a critical point: separation curves on s were constructed as closed polygons, then piecewise linear vector fields of the specified classification were automatically created. [20] put a number of restrictions onto the separation curves: all points on them had to have an F-classification of either inflow or outflow, and the separation curves had to be closed curves. Figures 3b-d show an example. However, as we will show later in this paper, separation curves on s can also be hyperbolic or elliptic, and they do not have to be closed.

3 EXTRACTING THE SECTORS AROUND A CRITICAL POINT

In this section we describe how to segment s into areas of different F-classification. We first assume that we know the location of a higher order critical point c in \mathbf{v} , such that a small closed surface s can be placed around it. However, in practice higher order critical points rarely appear because they are usually split into clusters of first order critical points. Our approach works for these cases as well: s is placed around the cluster, and in addition the location of c has to be set inside s . To do so, we either choose the average

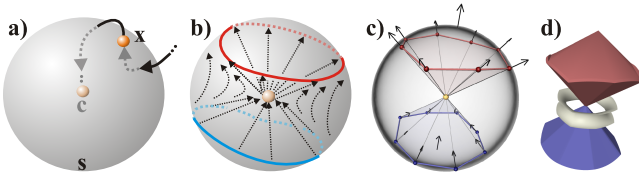


Figure 3: a) although $\mathbf{v}(\mathbf{x})$ points outside s , \mathbf{x} is part of an inflow sector; b) critical point consisting of two closed separation curves: outflow (red), and inflow (blue) separating three sectors; c) modelled closed polygons on s representing separation surfaces; d) final icon (from [20]).

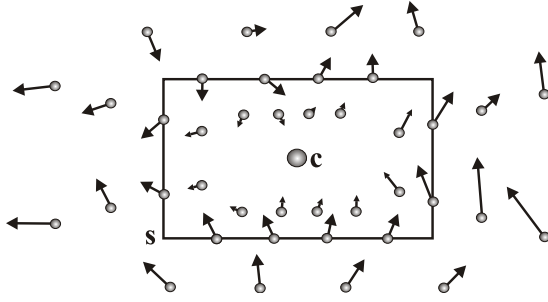


Figure 4: A vector field \mathbf{v} and a closed surface s with its center \mathbf{c} .

position of the critical in the cluster, or we simply choose the center of s . In fact, our approach can be applied to *any* region of \mathbf{v} giving a valid topological description of it.

The main contribution of this section is to show that the segmentation of s into areas of different F-classification essentially corresponds to the extraction of the topological skeleton of an appropriate 2D vector field \mathbf{u} on s where every critical point of \mathbf{u} is provided with an additional Bit of information. The segmentation of s is done entirely by sampling \mathbf{v} on s : the behavior of \mathbf{v} outside s is not considered. This approach is reflected by the introduction of a new 3D vector field \mathbf{w} which is a simplified version of \mathbf{v} : \mathbf{v} and \mathbf{w} coincide on s but may differ in other areas. We start with the introduction of \mathbf{u} and \mathbf{w} as well as some other auxiliary vector fields.

3.1 Auxiliary vector fields

Again, we consider a 3D vector field \mathbf{v} , a closed surface s in the domain of \mathbf{v} , and a point \mathbf{c} inside s . Here we use an axis-parallel box which simplifies the following implementations: vector operation on s become operations on a collection 2D plane vector fields. Figure 4 gives an illustration of a 2D example. Out of this, we define a number of auxiliary vector fields:

- Let $\mathbf{v}|_s$ be the restriction of \mathbf{v} to the domain s . This means that $\mathbf{v}|_s$ is a map from the 2D domain s to \mathbb{R}^3 . Figure 5a illustrates this. $\mathbf{v}|_s$ is the only part of \mathbf{v} which is used to classify \mathbf{c} .

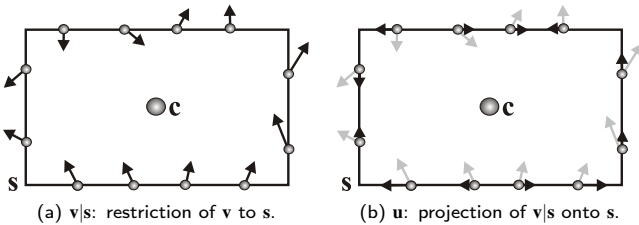


Figure 5: Restriction to and central projection onto s .

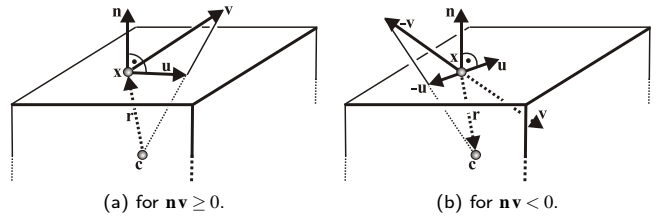


Figure 6: Obtaining the central projection vector field \mathbf{u} .

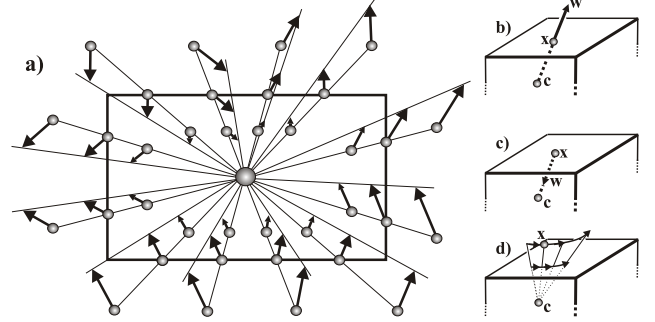


Figure 7: a) Auxiliary 3D vector field \mathbf{w} ; b) \mathbf{x} is a \mathbf{w} -outflow critical point of \mathbf{u} ; c) \mathbf{x} is \mathbf{w} -inflow critical point of \mathbf{u} ; d) the central projection of a stream line of \mathbf{w} is a stream line of \mathbf{u} .

- Let \mathbf{n} be the normalized outward normal at each point of s .
- Let \mathbf{u} be the central projection of $\mathbf{v}|_s$ onto s with the projection center \mathbf{c} . For every point $\mathbf{x} \in s$, $\mathbf{u}(\mathbf{x})$ can be computed as

$$\mathbf{u} = \alpha \mathbf{r} + \beta \mathbf{v}$$

with

$$\mathbf{r} = \text{sign}(\mathbf{n} \cdot \mathbf{v}) \cdot (\mathbf{x} - \mathbf{c})$$

$$\alpha = \frac{-(\mathbf{n} \cdot \mathbf{v})}{(\mathbf{n} \cdot \mathbf{r}) + (\mathbf{n} \cdot \mathbf{v})}, \quad \beta = \frac{(\mathbf{n} \cdot \mathbf{r})}{(\mathbf{n} \cdot \mathbf{r}) + (\mathbf{n} \cdot \mathbf{v})}.$$

Figure 6 explains this. Figure 5b illustrates \mathbf{u} for the 2D example.

- Let \mathbf{w} be constructed in the following way: given a point $\mathbf{x} \in \mathbb{R}^3$ with $\mathbf{x} \neq \mathbf{c}$, we intersect s with the line segment (\mathbf{x}, \mathbf{c}) . This gives a unique intersection point \mathbf{s}_x on s which can be written as $\mathbf{s}_x = (1 - \lambda_x) \mathbf{c} + \lambda_x \mathbf{x}$ for a certain $\lambda_x \geq 0$. Then we compute $\mathbf{w}(\mathbf{x}) = \mathbf{v}(\mathbf{s}_x) / \lambda_x$. In addition we set $\mathbf{w}(\mathbf{c}) = (0, 0, 0)^T$. Figure 7a illustrates the definition of \mathbf{w} .

Note that \mathbf{u} is a 2D vector field on the surface s , while \mathbf{v} and \mathbf{w} are 3D vector fields. \mathbf{w} can be considered as a simplified version of \mathbf{v} : \mathbf{v} and \mathbf{w} are identical on s , while all other vectors of \mathbf{w} are obtained by a linear interpolation between \mathbf{c} and a point on s . Since we only use $\mathbf{v}|_s$ for the classification, we are allowed to do the classification for \mathbf{w} instead for \mathbf{v} .

Due to the construction of \mathbf{u} and \mathbf{w} , there are a number of relations between them: $\mathbf{x} \in s$ is a critical point of \mathbf{u} iff $\mathbf{v}(\mathbf{x}) = \gamma(\mathbf{x} - \mathbf{c})$ for a certain $\gamma \neq 0$. In this case, the stream line of \mathbf{w} starting in \mathbf{x} is a straight line from \mathbf{x} to \mathbf{c} , either in forward or in backward integration. Hence, every critical point of \mathbf{u} can be classified by two criteria:

- concerning the classical topological classification of a critical point of a 2D vector field, i.e. as a source, sink, or saddle. (The structurally unstable case of a center is not considered here.)

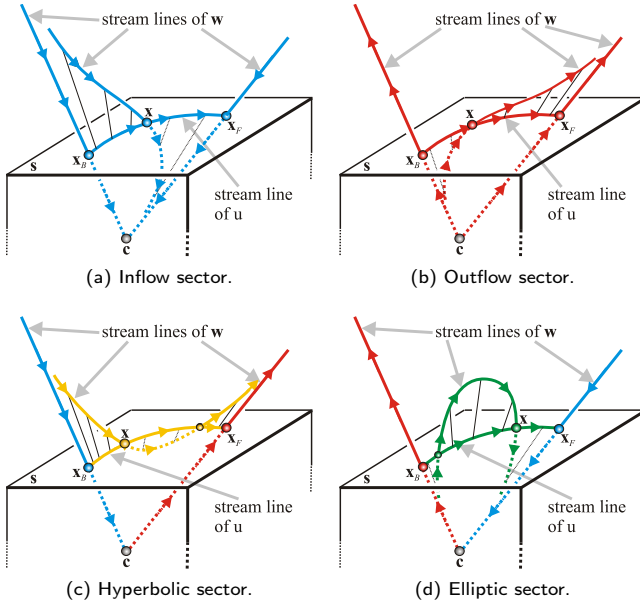


Figure 8: F-classification of a single point \mathbf{x} on s depends on the \mathbf{w} -inflow/outflow behavior of the end points of the stream line through \mathbf{x} in \mathbf{u} .

end point \mathbf{x}_B backward integration	end point \mathbf{x}_F forward integration	F-classification of \mathbf{x}
\mathbf{w} -inflow	\mathbf{w} -inflow	inflow
\mathbf{w} -outflow	\mathbf{w} -outflow	outflow
\mathbf{w} -inflow	\mathbf{w} -outflow	hyperbolic
\mathbf{w} -outflow	\mathbf{w} -inflow	elliptic

Table 2: F-classification of a single point \mathbf{x} on s .

- concerning the sign of γ : \mathbf{x} is called a \mathbf{w} -inflow point if $\gamma < 0$, i.e., $\mathbf{w}(\mathbf{x})$ points to \mathbf{c} . For $\gamma > 0$, \mathbf{x} is called a \mathbf{w} -outflow point. Figures 7b and 7c illustrate this.

Another relation between \mathbf{u} and \mathbf{w} can be established concerning their stream lines. Let $\mathbf{x} \neq \mathbf{c}$ be a point in the 3D domain of \mathbf{w} . Considering the stream line of \mathbf{w} starting in \mathbf{x} , it turns out that its central projection onto s is a stream line of \mathbf{u} . This follows directly from the definition of \mathbf{u} and \mathbf{w} . Figure 7d illustrates this relation.

3.2 F-classification of a single point on s

After establishing the relations between \mathbf{u} and \mathbf{w} , we can get the F-classification of an arbitrary point $\mathbf{x} \in s$ in a simple way. Instead of integrating \mathbf{w} starting from \mathbf{x} and observing whether or not the stream line ends in \mathbf{c} , we apply a 2D stream line integration of \mathbf{u} starting from \mathbf{x} . This integration ends in two certain critical points of \mathbf{u} : \mathbf{x}_B by backward and \mathbf{x}_F by forward integration. Usually \mathbf{x}_B is a source and \mathbf{x}_F is a sink, but they might be saddles as well – in case that \mathbf{x} lies on a separatrix of the topological skeleton of \mathbf{u} . However, the F-classification of \mathbf{x} can simply be obtained by considering the \mathbf{w} -inflow/outflow behavior of \mathbf{x}_B and \mathbf{x}_F respectively, as summarized in table 2 and illustrated in figure 8.

The goal of this paper is to segment s into areas of different F-classification. Since we are now able to F-classify any point on this surface, we could naively do so for a high number of sample points. In figure 9 we did this for a test data set (a region in the benzene data set, which will be explained in detail in section 5 – we use this test data set throughout the rest of this section for algorithmic

Figure 9: Naive approach of F-classifying s : 256^2 points on each face have been F-classified according to table 2 by integrating stream lines starting/ending in the depicted sources/sinks. Computation time: 700 seconds (P4 3.4GHz).

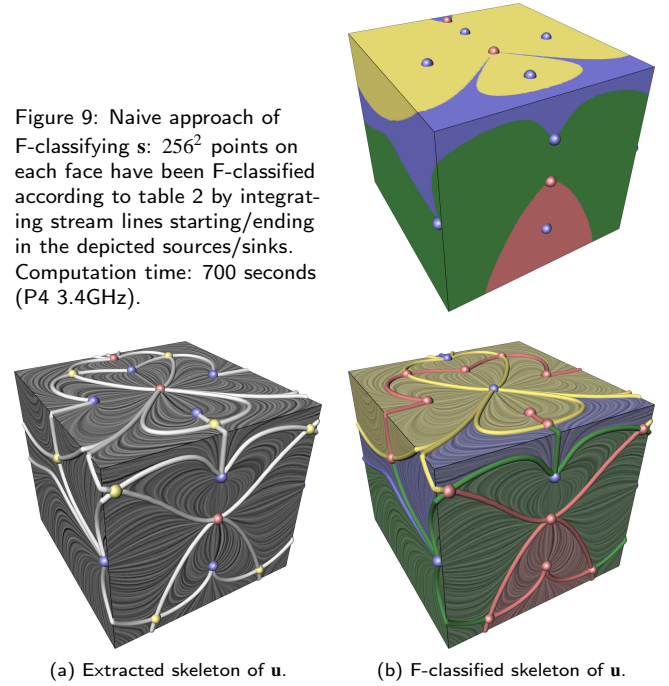


Figure 10: Exploiting the topology of \mathbf{u} to F-classify s .

explanations). It clearly shows distinctive areas of color coded flow behavior. There are three major reasons, why this approach is not satisfying:

- It takes a rather long time to integrate the stream lines for a reasonable resolution. In this example, we started a stream line integration at 256^2 sample points on each face of the box. This took more than 700 seconds on a Pentium 4 with 3.4 GHz.
- It only yields a visual representation of the different sectors. One still needs to apply some other algorithm in order to get a feature-based separation, i.e. lines or points.
- It does not capture all features on s . Even already for first order 3D saddles enclosed by s there are points and lines on the surface with a different F-classification than their surrounding area (hyperbolic area vs. inflow/outflow points and lines). Even for very high resolutions, such points and lines are only hit by accident.

In the following subsections we present an algorithm which captures all features of \mathbf{w} and is orders of magnitude faster.

3.3 F-classification of all points on s

For the F-classification of a single point, we utilized the stream line of \mathbf{u} through that point and looked at the \mathbf{w} -inflow/outflow behavior of its start and end point. Those start and end points are critical points of \mathbf{u} . It is easy to see, that all points \mathbf{x} have the same F-classification, if all their stream lines start and end in the same pair of critical points. Thus, the topological skeleton of \mathbf{u} gives the desired segmentation of s . We give the following algorithm:

- Extract the topological skeleton of \mathbf{u} . It consists of critical points and separation curves (Figure 10a).
- F-classify all critical points of \mathbf{u} concerning their \mathbf{w} -inflow/outflow property (Figure 10b).

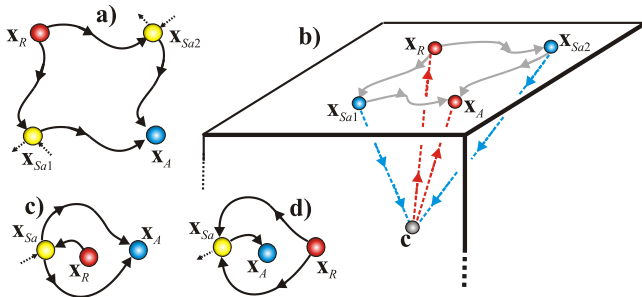


Figure 11: a) a topological substructure of \mathbf{u} consisting of a source \mathbf{x}_R (red), a sink \mathbf{x}_A (blue), two saddles $\mathbf{x}_{Sa1}, \mathbf{x}_{Sa2}$ (yellow), and 4 separatrices; b) classification of the topological segment on \mathbf{u} concerning the \mathbf{w} -inflow/outflow behavior of the critical points; c), d) other topological substructures of \mathbf{u} .

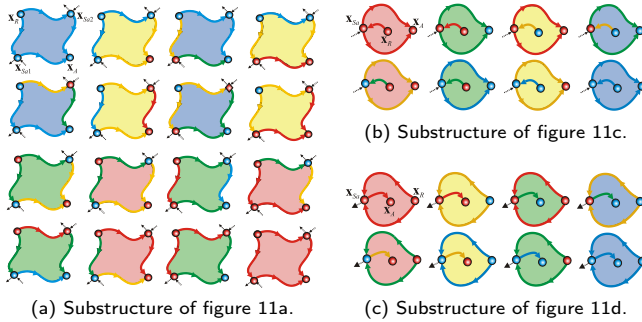


Figure 12: Cases for F-classifying the substructures of the topological skeleton of \mathbf{u} . Colored according to table 1.

3. F-classify all separatrices of \mathbf{u} . To do so, consider the \mathbf{w} -inflow/outflow property of the two critical points where the separatrix starts and ends (Figure 10b).
4. F-classify the remaining areas. To do so, consider the \mathbf{w} -inflow/outflow property of the two critical points where the integration in forward and backward direction starts and ends (Figure 10b).

We describe details of this algorithm at an example. Figure 11a shows a certain substructure of a topological skeleton of \mathbf{u} consisting of a source \mathbf{x}_R , a sink \mathbf{x}_A and two saddles $\mathbf{x}_{Sa1}, \mathbf{x}_{Sa2}$. From each saddle, two separatrices have been integrated (one in forward and one in backward direction) which end in \mathbf{x}_R and \mathbf{x}_A respectively. In our example we assume that $\mathbf{x}_R, \mathbf{x}_A$ are \mathbf{w} -outflow while $\mathbf{x}_{Sa1}, \mathbf{x}_{Sa2}$ are \mathbf{w} -inflow, as shown in figure 11b. Note that the color coding of figure 11b is different than figure 11a: here the red color means \mathbf{w} -outflow, and the blue color means \mathbf{w} -inflow. Then the separatrices from the source \mathbf{x}_R to both saddles have elliptic behavior, while the separatrices from both saddles to the sink \mathbf{x}_A possess hyperbolic behavior (see table 2). All points *inside* the area surrounded by the four separatrices have the property that a forward integration of \mathbf{u} starting from them ends in \mathbf{x}_A while a backward integration ends in \mathbf{x}_R . Hence they are part of an outflow sector (table 2).

3.4 A complete system of 2D topological substructures

The example of figures 11a-b shows that the elements (i.e., critical points, separatrices, inner area) of a topological substructure may have a different F-classification. Since the F-classification is entirely based on the \mathbf{w} -inflow/outflow behavior of the critical points, there are 16 cases of F-classifying this topological substructure with

4 critical points. Figure 12a illustrates this: the location of critical points is the same as in figure 11a for each of the cases. The color coding here corresponds to table 1 and gives the F-classification of the critical points, separatrices, and inner areas respectively.

Another possible topological substructure of \mathbf{u} is shown in figure 11c: both outflow separatrices of a saddle \mathbf{x}_{Sa} end in the same sink \mathbf{x}_A , whereas inside the surrounded area there is a source with a separatrix to the saddle as well. A similar substructure with exchanged source and sink is shown in figure 11d. Figures 12b-c show the F-classification of the 8 possible cases for each of those two types of substructures.

Finally we show that the topological substructures of figure 11 are essentially the only ones which can appear in \mathbf{u} . We do so by considering the following facts:

- Each topological substructure consists of exactly one source and one sink. In fact, the inner area of a substructure describes exactly the area where the flow goes from this source to this sink. If there were for instance two sources, we would have another separation between them.
- Each separatrix goes from a saddle to a source or a sink. This means that we do not allow structurally unstable saddle connections (i.e., stream lines from one saddle to another).
- Each source/sink must not have more than two separatrices of the substructure ending in it. If a source/sink had three separatrices ending in it, the middle one would define another separation.

From these points it follows that the maximal number of separatrices involved in a substructure is 4. This gives that at most two saddles can be involved. The only case with two saddles is shown in figure 11a, the two cases with one saddle are shown in figures 11c and 11d. There is also a trivial case with no saddles involved: if \mathbf{u} has only one source, one sink and no saddles, and the complete flow on \mathbf{u} goes from the source to the sink. In this case, the complete area of \mathbf{s} (except the critical points themselves) gets the F-classification concerning to the F-classification of the critical points.

3.5 Obtaining a minimal skeleton

In section 3.3 we extracted the topological skeleton of the projected 2D vector field \mathbf{u} . While these critical points and separation curves segment \mathbf{u} into areas of different flow behavior, not all of them are necessarily needed to do the segmentation into areas of different F-classification. A redundancy with respect to the segmentation of \mathbf{w} is introduced to that skeleton since only the \mathbf{w} -inflow/outflow behavior has to be considered in order to do the segmentation. In other words, some neighboring substructures of the 2D skeleton may have the same F-classification and thus, the separation between them does not reflect different sectors of F-classification. Figures 13a-b illustrate this.

A minimal skeleton representing the different sectors of the F-classification only has to be found: structural elements of the 2D skeleton with identical behavior as their neighbors have to be either merged with them or completely removed. For this, we convert the 2D skeleton into a graph representation, where critical points reflect nodes, separation curves correspond to edges between two nodes, and inner areas are represented by their associated curves and points. We consider a graph to emphasize that any geometrical information can be discarded for the following. To minimize the skeleton, we have to

- remove edges, if they exhibit the same F-classification as their neighboring areas,
- merge areas, if an edge belonging to all of them has been removed,

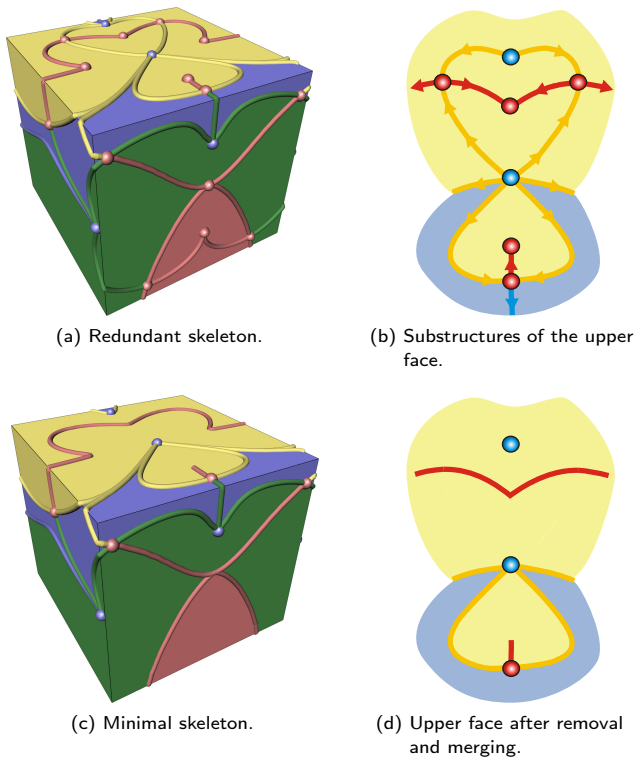


Figure 13: F-classified topological skeleton of \mathbf{u} before and after the removal of redundant elements.

- remove unconnected nodes (i.e., not connected to an undeleted edge), if they have the same F-classification as their surrounding area,
- remove nodes, if they possess the same F-classification as all their connected edges,
- merge two edges, if both have been connected to the same deleted node.

Figures 13c-d illustrate the outcome of this process. Note that nodes cannot be merged since they correspond to isolated critical points in the skeleton, and areas can not be removed since their union covers the whole 2D domain on s . The obtained graph represents the minimal skeleton needed to distinguish between sectors of different F-classification. Critical points in this skeleton correspond to directions of straight inflow/outflow, while the remaining curves give the separation surfaces in between the different sectors (i.e., areas).

Our algorithm needed 4 seconds on our hardware to extract, F-classify and minimize the skeleton of the test data set. This is much faster than the naive approach depicted in figure 9. Furthermore, our algorithm guarantees to capture all features on s . For example, figure 13c shows in contrast to figure 9 an outflow separation curve between two hyperbolic areas on the upper face.

4 ICONIC VISUALIZATION

To visualize a critical point, we place an appropriate icon into its location. Our approach is very similar to [20] with the difference that we do not put the restriction on the separation surfaces to be either inflow or outflow. Those surfaces are constructed from the remaining curves of the minimal skeleton by creating a triangle fan between the curve and the critical point c . To perceptually enhance

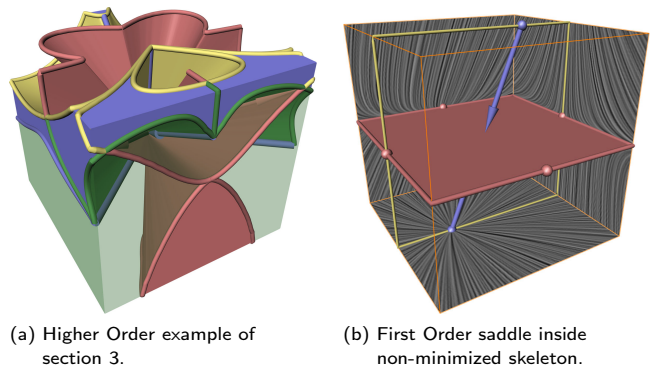


Figure 14: Icons.

their visualization, the curves on the box are displayed using cylindrical meshes. If a separation surface degenerates to a line (i.e., point in the skeleton denoting direction of straight inflow/outflow), we visualize it using a 3D arrow. Color coding is according to the F-Classification.

It remains to visually depict the sectors of different 3D flow behavior. Inflow/outflow sectors are represented by filling the areas with an opaque surface using the respective color. For elliptic sectors we do the same with a semi-transparent surface. Hyperbolic sectors are left open. Figure 14a shows the icon for the example used in section 3. In the end it turns out, that this visualization scheme yields icons for first order critical points similar to [16, 19] (Figure 14b).

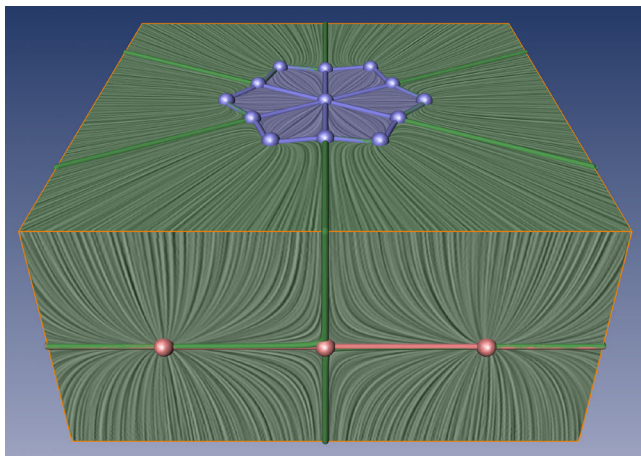
5 APPLICATIONS

Figures 1, 15 and 16 visualize the electrostatic field around a benzene molecule. This data set was calculated on a 101^3 regular grid using the fractional charges method described in [13]. Its topological richness is shown in figure 1a: it consists of 184 first order critical points.

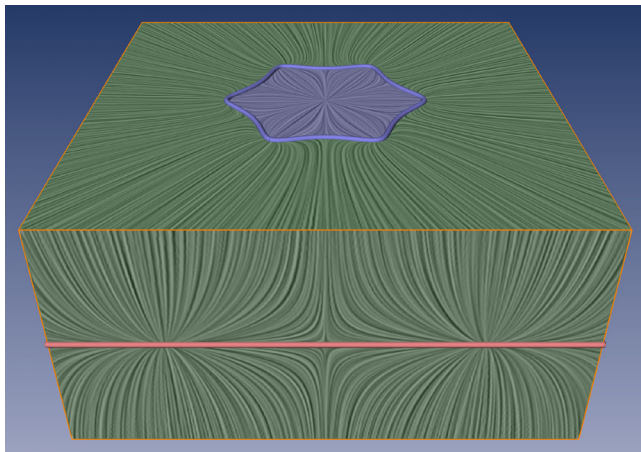
This field describes the force of the electrostatic potential of the benzene molecule upon a positive point charge given in a certain location. If such a point charge is situated very close to the molecule, the closest atom will exert the highest force on it, i.e., attract or repel it. The influence of a single atom decreases the farther the point charge is located from the whole molecule. Instead, all atoms have nearly the same influence. One might say that the molecule as a whole is exerting force on a somewhat far located point charge. Thus, it is possible to distinguish between a near and a far field. Furthermore, the critical points of the electrostatic field represent minima and maxima of the potential. See [1] for a further discussion of classifying atoms and molecules based on field topology.

These properties give a good setting for our algorithm. By placing a large box around the whole molecule, we yield a high level of abstraction. Figure 15a shows the box around the whole molecule together with the extracted and F-classified topological skeleton of the projected 2D vector field \mathbf{u} . The minimal skeleton is depicted in figure 15b. As it can be seen here, there is a star-shaped inflow area (blue), an outflow line (red), and an elliptic area (green) between them in the visible parts of the box. Figure 1b shows the icon for this area together with stream lines of \mathbf{w} . It clearly shows the behavior of the far field of the benzene molecule, if one compares it with figure 15c.

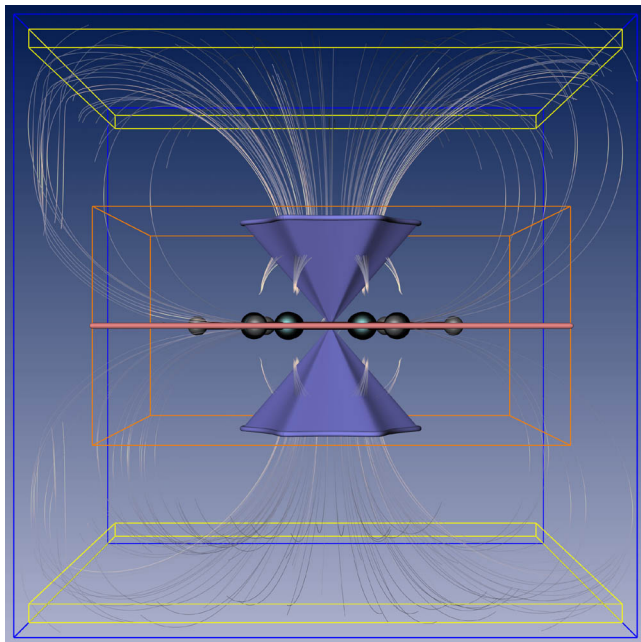
In figure 16 we lowered the abstraction level by subdividing the domain in 3 (figure 16a) or 9 (figure 16b-c) subareas. This clearly shows the presence of a more complex topological behavior if we zoom into regions of interest. This is due to the fact that these de-



(a) Extracted and F-classified skeleton.



(b) Minimal skeleton.



(c) Icon. Stream lines of the original vector field have been seeded inside the yellow boxes at the bottom and top.

Figure 15: Benzene data set: High level of topological abstraction.

tailed regions are governed by the near field because the influence of the individual atoms increases. Figure 16 shows that topologically rather complex structures are present which consist of complex areas of different F-classification.

The application of our technique to this topologically complex data set shows its usefulness at various levels of simplification: if a large area of interest is chosen, a rough global topological impression about the global behavior of the vector field can be obtained. Focusing the area of interest to particular smaller areas inside, topologically more complex structures become visible and provide a deeper insight into the topological behavior of the vector field.

6 CONCLUSIONS

In this paper we made the following contributions:

- We presented a method to segment the regions around a higher order critical point into areas of different 3D flow behavior (F-classification).
- We showed that this segmentation can be done by extracting and minimizing the topological skeleton of a 2D vector field on a closed surface circumscribing the critical point. For this, each critical point of the 2D vector field had to be equipped with an additional Bit of information.
- We represented the segmentation of the areas around a 3D higher order critical point by an appropriate icon.
- We applied the method not only to analyze the topological behavior around higher order critical points but to any area of interest, e.g., around clusters of critical points. This way we have a topological simplification tool for 3D vector fields by replacing the topological skeleton inside the area of interest by the created icon.
- We applied the topological simplification approach to a topologically complex test data set.

There are a number of issues left for future research:

- Our current approach is based on the assumption that the complete topological segmentation of \mathbf{u} is given by critical points and separatrices starting from them. However, there may also be isolated closed stream lines on \mathbf{u} which topologically act as sources or sinks. This tends to happen when a swirling behavior of \mathbf{v} inside \mathbf{s} is present, making the approach in the presented form fail. The additional consideration of isolated closed stream lines on \mathbf{u} is intended to be included into the approach.
- The approach can be extended to work on areas with critical lines passing through.
- Although for 2D vector fields there is a simple relation between the number of sectors of different flow behavior around a higher order critical point and its index [4], we are not aware yet of a similar relation for the 3D case.

ACKNOWLEDGEMENTS

We thank Jan Reininghaus for his great implementational efforts. All visualizations in this paper have been created using AMIRA – a system for advanced visual data analysis [14] (see <http://amira.zib.de/>).

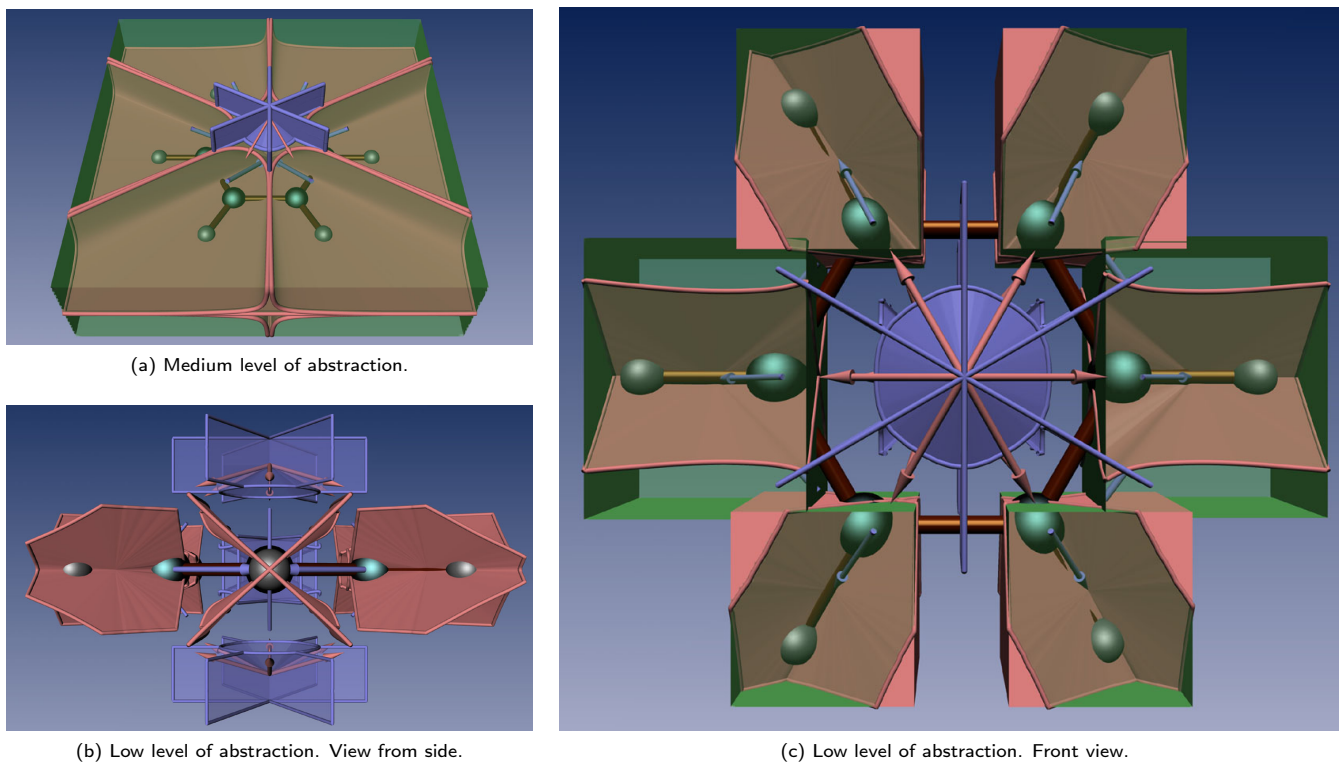


Figure 16: Benzene data set: Medium and low level of abstraction.

REFERENCES

- [1] R.F.W. Bader. *Atoms in Molecules - A Quantum Theory*. Oxford University Press, Oxford, 1990.
- [2] W. de Leeuw and R. van Liere. Collapsing flow topology using area metrics. In *Proc. IEEE Visualization '99*, pages 349–354, 1999.
- [3] W. de Leeuw and R. van Liere. Visualization of global flow structures using multiple levels of topology. In *Data Visualization 1999. Proc. VisSym 99*, pages 45–52, 1999.
- [4] P.A. Firby and C.F. Gardiner. *Surface Topology*, chapter 7, pages 115–135. Ellis Horwood Ltd., 1982. *Vector Fields on Surfaces*.
- [5] A. Globus, C. Levit, and T. Lasinski. A tool for visualizing the topology of three-dimensional vector fields. In *Proc. IEEE Visualization '91*, pages 33–40, 1991.
- [6] J. Helman and L. Hesselink. Representation and display of vector field topology in fluid flow data sets. *IEEE Computer*, 22(8):27–36, August 1989.
- [7] S.K. Lodha, J.C. Renteria, and K.M. Roskin. Topology preserving compression of 2D vector fields. In *Proc. IEEE Visualization 2000*, pages 343–350, 2000.
- [8] H. Löffelmann, H. Doleisch, and E. Gröller. Visualizing dynamical systems near critical points. In *Spring Conference on Computer Graphics and its Applications*, pages 175–184, Budmerice, Slovakia, 1998.
- [9] K. Mahrous, J. Bennett, G. Scheuermann, B. Hamann, and K. Joy. Topological segmentation in three-dimensional vector fields. *IEEE Transactions on Visualization and Computer Graphics*, 10(2):198–205, 2004.
- [10] S. Mann and A. Rockwood. Computing singularities of 3D vector fields with geometric algebra. In *Proc. IEEE Visualization 2002*, pages 283–289, 2002.
- [11] F.H. Post, B. Vrolijk, H. Hauser, R.S. Laramée, and H. Doleisch. The state of the art in flow visualization: Feature extraction and tracking. *Computer Graphics Forum*, 22(4):775–792, 2003.
- [12] G. Scheuermann, H. Krüger, M. Menzel, and A. Rockwood. Visualizing non-linear vector field topology. *IEEE Transactions on Visualization and Computer Graphics*, 4(2):109–116, 1998.
- [13] D. Stalling and T. Steinke. Visualization of vector fields in quantum chemistry. Technical report, ZIB Preprint SC-96-01, 1996. <ftp://ftp.zib.de/pub/zib-publications/reports/SC-96-01.ps>.
- [14] D. Stalling, M. Westerhoff, and H.-C. Hege. Amira: A highly interactive system for visual data analysis. *The Visualization Handbook*, pages 749–767, 2005.
- [15] H. Theisel. Designing 2D vector fields of arbitrary topology. *Computer Graphics Forum (Eurographics 2002)*, 21(3):595–604, 2002.
- [16] H. Theisel, T. Weinkauff, H.-C. Hege, and H.-P. Seidel. Saddle connectors - an approach to visualizing the topological skeleton of complex 3D vector fields. In *Proc. IEEE Visualization 2003*, pages 225–232, 2003.
- [17] X. Tricoche, G. Scheuermann, and H. Hagen. A topology simplification method for 2D vector fields. In *Proc. IEEE Visualization 2000*, pages 359–366, 2000.
- [18] X. Tricoche, G. Scheuermann, and H. Hagen. Continuous topology simplification of planar vector fields. In *Proc. Visualization 01*, pages 159–166, 2001.
- [19] T. Weinkauff, H. Theisel, H.-C. Hege, and H.-P. Seidel. Boundary switch connectors for topological visualization of complex 3d vector fields. In *Data Visualization 2004. Proc. VisSym 04*, 2004.
- [20] T. Weinkauff, H. Theisel, H.-C. Hege, and H.-P. Seidel. Topological construction and visualization of higher order 3D vector fields. *Computer Graphics Forum (Eurographics 2004)*, 23(3):469–478, 2004.
- [21] R. Westermann, C. Johnson, and T. Ertl. Topology-preserving smoothing of vector fields. *IEEE Transactions on Visualization and Computer Graphics*, 7(3):222–229, 2001.
- [22] T. Wischgoll and G. Scheuermann. Detection and visualization of closed streamlines in planar flows. *IEEE Transactions on Visualization and Computer Graphics*, 7(2):165–172, 2001.